Calculations of structure and IR-spectrum for small UF_6 clusters

T. A. Beu
University ''Babeş-Bolyai,'' Department of Theoretical Physics, 3400 Cluj-Napoca, Romania

J. Onoe and K. Takeuchi
The Institute of Physical and Chemical Research (RIKEN), Wako-shi, 351-01 Saitama, Japan

(Received 4 December 1996; accepted 8 January 1997)

A new site–site intermolecular potential model for UF_6, featuring exchange, dispersion, electrostatic and induction terms, is presented. The new potential, with the parameters adjusted according to the observed monomer transition dipole moment and reproducing the experimental temperature dependence of the second virial coefficient, is used to determine UF_6 cluster structures up to the hexamer and, by means of a second order line shift formalism, to calculate the corresponding IR-spectra in the region of the ν_3 vibrational mode (at 627.724 cm^{-1}). The contributions of the various potential terms to the frequency shifts are analyzed and the leading interaction mechanism is found to be the resonant dipole–dipole coupling. The theoretical spectra are compared and interpreted against recent Fourier transform IR-spectroscopy measurements. © *1997 American Institute of Physics.* [S0021-9606(97)02014-X]

I. INTRODUCTION

Through the frequency shift in the IR absorption of the UF_6 monomer, UF_6 cluster formation is considered to adversely affect selectivity in molecular laser isotope separation with the supersonic expansion technique. Due to the similarities between UF_6 and the less demanding SF_6 system, there has been quite great experimental and theoretical interest over the last two decades in the SF_6 clusters,[1–7] used to establish adequate experimental and theoretical approaches. Nevertheless, despite the importance of knowledge about formation kinetics and the frequency shift in the IR-spectrum of the UF_6 clusters, there have been no published results on this subject for a long time.

The only available experimental data are the recent FTIR spectroscopy measurements of Tanimura *et al.*,[8] which will subsequently be used as experimental counterpart for our calculations. The FTIR spectroscopic measurements in supersonic free jets have the advantage of a wider spectral coverage than any laser system, allowing for simultaneous observation of the spectra for both the monomer and the clusters.[8,9] Nevertheless, the absence of a size selection mechanism makes interpretation of the FTIR spectra quite difficult.

Recently we have reported a new site–site intermolecular potential for SF_6,[7] and the structures obtained by using it for small clusters up to the hexamer. By employing a newly developed second order perturbation approach, we have also evaluated the corresponding frequency shifts of the ν_3 vibrational monomer mode. The formalism consistently treats the degeneracy of the cluster states emerging from the identity of the constituent monomers and also takes into account the degeneracy of the monomer vibrational states. The underlying idea, extracted from early publications of Buckingham[10] concerning the frequency shifts in the IR or Raman spectra of chromophores under the influence of a solvent, is to treat the anharmonic contributions to the intramolecular force field and the intermolecular potential as a quantum mechanical perturbation of the molecular vibrations.

Basically, we attempted to follow the pattern used for the construction of the SF_6 intermolecular potential to establish the site–site intermolecular potential of UF_6, by fitting it to the observed temperature dependence of the second virial coefficient and by choosing appropriate effective charges of the interaction sites, consistent with the experimental monomer transition dipole moment.[11] However, due to the lack of a reliable U–U potential in the literature, the UF_6 intermolecular potential model and the overall strategy had to be adapted. Built into the total UF_6–UF_6 potential, with the fluorine data taken from our published SF_6–SF_6 potential,[7] the most elaborate available U–U potential of Pepper and Bursten[12] yields by far unreasonable virial coefficient and dimer structure. Consequently, we have resorted to fitting the potential coefficients for uranium, too. For this purpose we have enlarged the set of data to be reproduced by the intermolecular potential, including the equilibrium dimer separation as prescribed by the recommended isotropic UF_6–UF_6 potential of Aziz and Taylor.[13]

The adjusted UF_6–UF_6 potential is used to determine UF_6 cluster structures up to the hexamer, for which the IR-spectrum in the region of the ν_3 mode (at 627.724 cm^{-1}) is calculated by means of our previously published perturbational frequency shift approach, briefly described in Sec. II A.

The potential model we employ to determine the geometrical structures and line shifts of the SF_6 clusters, comprising exchange, dispersion, electrostatic and induction contributions, is described in Sec. II B.

Basic input data for the cluster structure and frequency shift calculations (the harmonic monomer frequencies, the displacement $\tilde{l}$-matrix, and the transformed cubic force constants ϕ_{rst}) are derived as part of the normal mode analysis of the monomer. Accurate treatment of UF_6 monomer spectroscopy implies the refinement of the intramolecular force field and the results of this approach, as well as the transformation principles of the cubic force constants of UF_6 from valence to normal coordinates, are presented in Sec. III A.

 0021-9606/97/106(14)/5910/10/$10.00

Details of the adjustment procedure of the intermolecular potential parameters are described in Sec. III B. In order to establish the importance of the induction coupling in the case of the UF_6 clusters, we employ two variants of our potential model: One neglecting the induction interactions, hereafter referred to as ''potential I,'' and the other one including them, hereafter called ''potential II.''

Section III C is devoted to the description of the structures we have obtained for the UF_6 clusters ranging from dimer to hexamer by using the two variants of the new potential model.

In Sec. III D, the results of our frequency shift calculations are described in detail. The contributions to the frequency shifts from the various interaction mechanisms are analyzed and the theoretical spectra are compared with the experimental evidence. The appropriateness of the inclusion of the induction interactions in the potential model is also discussed.

II. THEORETICAL MODEL

A. Perturbation approach for cluster frequency shifts

In this section we will outline the main results of our previously published second order perturbation approach for cluster frequency shifts.[7]

The total cluster Hamiltonian may be written as

$$H=\frac{hc}{2}\sum_{r=1}^{3N-6}\sum_{m=1}^{M}\omega_r(p_{rm}^2+q_{rm}^2)+\frac{hc}{6}\sum_{r,s,t=1}^{3N-6}\sum_{m=1}^{M}\phi_{rst}q_{rm}q_{sm}q_{tm}+U, \tag{1}$$

where the first sum describes the uncoupled harmonic oscillations, the second sum is the anharmonic correction, while U represents the intermolecular potential. Here ω_r and ϕ_{rst} are the harmonic frequencies and the cubic force constants in units of wave numbers, respectively. q_{rm} and p_{rm} are position and momentum operators associated with the normal mode r of molecule m. M stands for the number of identical N-atomic molecules. The first two sums of Hamiltonian (1) describe the conventional normal mode approach for the individual molecules including cubic anharmonicities.

In view of the fact that Hamiltonian (1) is dominated by the harmonic term (first sum), which in addition allows for a full analytical diagonalization, providing a basis set for the Hilbert space of the cluster states, the anharmonic term and the intermolecular potential can be treated as a perturbation

$$W=\frac{hc}{6}\sum_{r,s,t=1}^{3N-6}\sum_{m=1}^{M}\phi_{rst}q_{rm}q_{sm}q_{tm}+U. \tag{2}$$

Within the framework of the stationary perturbation theory,[14] both the first and second order energy corrections are expressed in terms of the perturbation matrix elements, given by

$$W_{ni,n'i'}\equiv\langle 1_{ni}|W|1_{n'i'}\rangle=\left(U_0+\frac{1}{4}\sum_r\sum_m\frac{\partial^2U}{\partial q_{rm}^2}\right)\delta_{nn'}\delta_{ii'}+\frac{1}{2}\frac{\partial^2U}{\partial q_{ni}\partial q_{n'i'}},$$

where $|1_{ni}\rangle$ denotes the total cluster state in which the nth normal mode of the ith molecule is simply excited. For a degenerate monomer normal mode $n\in\Gamma$, where Γ is the subspace of the considered normal mode.

Defining the reduced perturbation matrix elements

$$\tilde{W}_{ni,n'i'}=\frac{1}{2}\frac{\partial^2U}{\partial q_{ni}\partial q_{n'i'}}, \tag{3}$$

the corresponding eigenvalue problem,

$$\sum_{n'\in\Gamma}\sum_{i'=1}^{M}[\tilde{W}_{ni,n'i'}-hc\Delta\nu_{ni}^{(1)}\delta_{nn'}\delta_{ii'}]c_{n'i',ni}=0,\quad n\in\Gamma,\quad i=1,2,\ldots,M, \tag{4}$$

directly yields the first order frequency shifts $\Delta\nu_{ni}^{(1)}$ for the fundamental excitation from the ground state to the simply excited levels E_{ni}. As is apparent from definition (3) of the reduced perturbation matrix elements, the first order line shifts are independent of the intramolecular force constants, depending only on the curvature of the intermolecular potential. The diagonalization of the reduced perturbation matrix provides, besides the first order frequency shifts, the coefficients $c_{ni,n'i'}$ (as eigenvector components), which satisfy the completeness relation $\Sigma_{n'\in\Gamma}\Sigma_{i'}|c_{n'i',ni}|^2=1$, and which further enter the expressions of the second order line shifts.

The second order line shift, $\Delta\nu_{ni}^{(2)}$, may be cast in the form

$$\Delta\nu_{ni}^{(2)}=\sum_{n',n''\in\Gamma}\sum_{i',i''}c_{n'i',ni}c_{n''i'',ni}^{*}\Delta\nu_{n'i',n''i''}^{(2)}, \tag{5}$$

where

$$\Delta\nu_{n'i',n''i''}^{(2)}=-\frac{\delta_{n'n''}\delta_{i'i''}}{4hc}\sum_r\frac{3-\delta_{rn'}}{\omega_r}\frac{\partial U}{\partial q_{ri'}}\phi_{n'n'r}-\frac{(1-\delta_{n'n''})\delta_{i'i''}}{8hc}\sum_r\frac{4+\delta_{rn'}+\delta_{rn''}}{\omega_r}\frac{\partial U}{\partial q_{ri'}}\phi_{n'n''r}+\frac{1}{4(hc)^2}\sum_{r\notin\Gamma}\sum_m\frac{1}{\omega_n-\omega_r}\frac{\partial^2U}{\partial q_{n'i'}\partial q_{rm}}\frac{\partial^2U}{\partial q_{n''i''}\partial q_{rm}}-\frac{1}{4(hc)^2}\sum_r\sum_m\frac{1}{\omega_n+\omega_r}\frac{\partial^2U}{\partial q_{n'i'}\partial q_{rm}}\frac{\partial^2U}{\partial q_{n''i''}\partial q_{rm}}. \tag{6}$$

Generally, the most significant contributions to the second order line shifts are due to the first term of Eq. (6), coupling the generalized intermolecular forces $-\partial U/\partial q_{ri'}$ with the intramolecular force constants $\phi_{n'n'r}$. It is noteworthy that the second order shifts do not depend on *all* cubic force constants, but only on those implying states belonging to subspace Γ of the considered normal mode.

The total frequency shift of a particular cluster spectral band obviously results from the sum of the corresponding first and second order shifts: $\Delta\nu_{ni}=\Delta\nu_{ni}^{(1)}+\Delta\nu_{ni}^{(2)}$.

The relative importance of the cluster spectral lines corresponding to a particular vibrational mode can be judged on the basis of the transition strength, which can be calculated as the squared cluster transition dipole moment weighted by the degeneracy of the cluster state. The Cartesian component for direction α of the cluster transition dipole moment is given by the approximate expression

$$\mu_{01}^{\alpha}=\frac{1}{\sqrt{2}}\sum_{n'\in\Gamma}\sum_{m}\left[\sum_{a}q_a\sum_{\alpha'}A_{\alpha\alpha'}^{m}\tilde{l}_{a\alpha'}^{n'}\right]c_{n'm,ni}^{*}, \tag{7}$$

where q_a is the charge associated with atom (site) a, $A_{\alpha\alpha'}^{m}$ is the rotation matrix which characterizes the position of molecule m in the cluster, and $\tilde{l}_{a\alpha'}^{n'}$ are elements of the displacement $\tilde{l}$-matrix, which results from the normal mode analysis of the monomer.

B. The intermolecular potential model

The functional form of the intermolecular potential we have chosen for calculating the structures of the UF_6 clusters and the corresponding vibrational frequencies shifts is the one we have previously used in the calculations for the SF_6 clusters,[7] and it comprises exchange, dispersion, electrostatic, and induction terms. A similar model was employed by van Bladel *et al.*[5] for SF_6, SiF_4, and SiH_4 dimer calculations. One of the important features of this potential type is that being based on site–site interactions, it depends on the relative atom positions, thus implicitly depending on the internal monomer vibrational coordinates.

The repulsive exchange and the attractive dispersion interactions are represented by standard (exp-6) terms:

$$U^{\mathrm{exch}}=\sum_{m=1}^{M-1}\sum_{m'=m+1}^{M}\sum_{i\in m}\sum_{j\in m'}A_{ij}\exp(-B_{ij}r_{ij}), \tag{8}$$

and

$$U^{\mathrm{disp}}=-\sum_{m=1}^{M-1}\sum_{m'=m+1}^{M}\sum_{i\in m}\sum_{j\in m'}\frac{C_{ij}}{r_{ij}^{6}}, \tag{9}$$

respectively, where r_{ij} is the distance between atom i belonging to monomer m and atom j belonging to monomer m'. The electrostatic term

$$U^{\mathrm{elec}}=\sum_{m=1}^{M-1}\sum_{m'=m+1}^{M}\sum_{i\in m}\sum_{j\in m'}\frac{q_iq_j}{r_{ij}} \tag{10}$$

implies the effective charges q_i placed on the atoms, such as to account for the vibrational transition dipole moment of the monomer.

The induction potential is generally composed of three-body terms describing the interaction between the charge q_j from molecule m' and the dipole induced at site i of molecule m by the charge q_k from molecule m''. In a simplified writing, evidencing the total induction field, the induction potential may be conveniently described as:

$$U^{\mathrm{ind}}=-\frac{1}{2}\sum_{m=1}^{M}\sum_{i\in m}\alpha_i\left|\sum_{\substack{m'=1\\m'\neq m}}^{M}\sum_{j\in m'}\frac{q_j\hat{\mathbf{r}}_{ij}}{r_{ij}^{2}}\right|^{2}, \tag{11}$$

where α_i is the polarizability of site i.

In our calculations, we employ two variants of the above potential model: The first one, designated in what follows as ''potential I,'' does not include the induction term, while the second, denoted as ''potential II,'' includes all the interactions.

III. RESULTS AND DISCUSSION

A. Intramolecular force field of UF_6

For the evaluation of the intermolecular potential derivatives with respect to the vibrational coordinates ($\partial U/\partial q_{rm}$, $\partial^2U/\partial q_{rm}^2$, and $\partial^2U/\partial q_{rm}\partial q_{sl}$) occurring in the frequency shift expressions, the so-called $\tilde{l}$-matrix of the monomer is needed.[7] The $\tilde{l}$-matrix describes the linear relationship between the Cartesian displacement and the normal coordinates of the atoms and results as part of the normal mode analysis of the monomer, performed according to the well-known G-F method of Wilson.[15] The $\tilde{l}$-matrix (besides the cubic force constants ϕ_{rst}) thus models the coupling between the intra- and intermolecular force fields.

The UF_6 monomer conforms to the O_h symmetry and, according to the irreducible representations of the O_h point group,[16] such a structure gives rise to one nondegenerate type A_{1g} vibration (ν_1), one doubly degenerate type E_g vibration (ν_2), two coupled triply degenerate type F_{1u} vibrations (ν_3, ν_4), one triply degenerate type F_{2g} vibration (ν_5), and one triply degenerate type F_{2u} vibration (ν_6). The F_{1u} vibrations are IR-active, while the A_{1g}, E_g, and F_{2g} vibrations are Raman active. The symmetry coordinates corresponding to the above symmetry species are described by Pistorius.[17]

In our calculations on the UF_6 monomer, we have employed the U–F bond length of 1.9962 Å and the quadratic intramolecular force field reported by Aldridge *et al.*[18] Regarding the force field, the accuracy of the listed symmetry force constants F_{11}, F_{22}, F_{33}, F_{34}, F_{44}, F_{55}, and F_{66} is not sufficient to allow for the observed frequencies to be exactly reproduced. Moreover, since the second order frequency shifts of the ν_3 vibrational mode of UF_6, on which we focus in this work, typically amount to several tenths of a cm^{-1}, as will be shown in Sec. III D, implying the decimal digits of the resulting frequencies, a previous refinement of the force constants provided by Aldridge *et al.* is necessary. The re-

TABLE I. Experimental vibrational frequencies ν_i [Aldridge *et al.* (Ref. 18)] and refined quadratic symmetry force constants F_{ij} for the UF_6 monomer.

i	Γ_i	ν_i (cm^{-1})	F_{ij} (mdyn/Å)	
1	A_{1g}	668.2	4.997 89	
2	E_g	534.5	3.197 93	
3,4	F_{1u}	627.724	3.725 75	
		187.5	0.096 46	0.160 00
5	F_{2g}	201.0	0.113 06	
6	F_{2u}	143.0	0.114 93	

finement procedure was accomplished using the ASYM20 program of Hedberg and Mills[19] and the resulting force constants are listed, along with the observed frequencies, in Table I.

In Table II we give the $\tilde{l}$-matrix elements yielded by the normal mode analysis of the UF_6 monomer, and corresponding to one of the substates of the threefold degenerate ν_3 mode (for the two other substates, the same non-zero elements occupy the y and z columns, respectively). They should be regarded as Cartesian displacements of the implied atoms for the unitary increment of the normal coordinate.

The transformation of the force constants from symmetry to normal coordinates, yielding the cubic force constants ϕ_{rst} which enter the expressions of the second order line shifts, was done by the L-tensor method of Hoy and coworkers.[20] The internal valence (or symmetry) coordinates R_i can be expressed in terms of normal coordinates Q_r by a non-linear transformation

$$R_i=\sum_r L_i^r Q_r+\sum_{r,s} L_i^{rs} Q_r Q_s+\sum_{r,s,t} L_i^{rst} Q_r Q_s Q_t+\cdots,$$

where the elements of the L-tensor, L_i^r, L_i^{rs}, L_i^{rst}, $\cdots$, have to be interpreted as first, second, and third order derivatives of the internal coordinate R_i with respect to the normal coordinates. In particular, the formula for the transformation of the cubic force constants from symmetry to normal coordinates is:

$$\phi_{rst}=\sum_{i,j,k} F_{ijk} L_i^r L_j^s L_k^t+\sum_{i,j} F_{ij}(L_i^{rs} L_j^t+L_i^{rt} L_j^s+L_i^{st} L_j^r).$$

Since for the UF_6 monomer only quadratic symmetry force constants, F_{ij}, are available, the transformed cubic force constants ϕ_{rst} merely account for the nonlinearity of the transformation of the quadratic force field of the monomer from symmetry to normal coordinates.

TABLE II. Displacement $\tilde{l}$-matrix for the ν_3 mode of the UF_6 monomer (in Å).

	$\tilde{l}_x$	$\tilde{l}_y$	$\tilde{l}_z$
U atom	−0.005 95	0	0
Axial F atoms	0.034 46	0	0
Equatorial F atoms	0.001 42	0	0

B. Intermolecular potential adjustment

In order to make our UF_6–UF_6 potential models (potential I, neglecting the induction interactions, and potential II, including them) as realistic as possible, we have adjusted their parameters in accordance with two macroscopic aspects: The transition dipole moment of the monomer and the temperature dependence of the second virial coefficient.

Our first concern in modeling the intermolecular potentials was to choose the effective atomic charges q_i in such a way as to reproduce the observed transition strength of the ν_3 vibration of the UF_6 monomer. As a reference for determining the effective atomic charges for both our potential models, we have considered the transition dipole moment value $\mu_{01}=0.385$ D of Kim and Person.[11] The effective charges result from the expression of the monomer transition dipole moment,

$$\mu_{01}^{\alpha}=\frac{1}{\sqrt{2}}\sum_a q_a \tilde{l}_{a\alpha}^n, \tag{12}$$

by imposing the additional condition of monomer neutrality. In the above relation a is the atom index and α is the Cartesian coordinate index. The components $\tilde{l}_{a\alpha}^n$ of the $\tilde{l}$-matrix are given in Table II. Thus, one obtains for the effective charges of the fluorine and uranium atoms the values $-1.027e$ and $6.165e$, respectively, implying a complete transfer of more than one electron from the uranium atom to each fluorine atom. This is obviously unphysical and incompatible with the partially covalent character of the U–F bond. It is apparent that additional ''electronic'' sites have to be defined on the U–F bonds, which are supposed to account for the six valence electrons of uranium ($5f^3 6d^1 7s^2$) and to carry the large effective charges suggested by the transition dipole moment.

A useful hint for the approximate position of the electronic sites along the U–F bond is provided by the maxima of the radial wave functions of the uranium valence atomic orbitals in the relativistic calculations of Onoe *et al.*[21] Since the positions of these maxima extend to about 1.35 Å from the uranium atom along the U–F bonds, we have taken this value as an initial guess for the position of the electronic sites, assigning them the physical effective charge $-1e$, slightly lower than the value resulted from Eq. (12). Correspondingly, the effective charge of uranium was taken $6e$. Although we have also investigated the effect of other site positions on the outcome of our virial coefficient, structure and IR-spectrum calculations, the most consistent results have been obtained by using the value of 1.35 Å, which defines both our potential models.

Because no $\tilde{l}$-matrix elements are available for the electronic sites, we have chosen to assign them the $\tilde{l}_{a\alpha}^n$ components of the neighboring fluorine atoms, implying for the ν_3 mode of UF_6 the parallel in phase vibration of the electronic sites with the fluorine atoms. The described choice of the effective charges q_a and the $\tilde{l}_{a\alpha}^n$ components for the electronic sites results, according to Eq. (12), in the value

TABLE III. Parameters of the intermolecular potential models for UF_6 (d_{xU} is the distance from a particular site to the U atom along the bond on which the former is located).

Potential model	Site	d_{xU}(Å)	A_{ii} (kJ/mol)	B_{ii} (Å^{-1})	C_{ii} (kJ/mol Å^6)	$q_i(e)$	α_i(Å^3)
Potential I	U		2 560 200	2.642	89 850	6	
	F	1.9962	336 133	4.128	665.9	0	
	e^-	1.3500	0	0	0	−1	
Potential II	U		2 560 200	2.642	89 850	6	7.9338
	F	1.9962	336 133	4.128	665.9	0	0.7557
	e^-	1.3500	0	0	0	−1	0

0.375 D for the monomer transition dipole moment, in fair agreement with the experimental value of Kim and Person.[11]

Since the charges assigned to the electronic sites, as well as their positions originate in considerations about the monomer transition dipole moment, they can be employed in both our potential models.

The coefficients A_{ij}, B_{ij}, and C_{ij}, defining the exchange and dispersion potentials given by Eqs. (8) and (9), can in principle be constructed from the coefficients A_{ii}, B_{ii}, and C_{ii} of the individual atomic species by applying the standard combination rules, $A_{ij}=\sqrt{A_{ii}A_{jj}}$, $B_{ij}=(B_{ii}+B_{jj})/2$, and $C_{ij}=\sqrt{C_{ii}C_{jj}}$. However, there is a tremendous difference between the availability of data on fluorine, on one hand, and uranium, on the other.

As regards fluorine, for A_{ii} and B_{ii}, describing the short range repulsive atom–atom interactions, we have considered the values obtained by Spackman[22] from fits to accurate calculations based on the Gordon–Kim electron gas model.[23] For the dispersion coefficients C_{ii}, describing the long range interaction of two non-polar species, we use the values we have obtained by fitting the temperature dependence of the second virial coefficient of SF_6 to experimental data.[7]

As for uranium, the most elaborate and presumably accurate U–U potential available in the literature is the one reported by Pepper and Bursten.[12] However, due to its very high binding energy (160 kJ/mol), any attempt to include an exp-6 fit of this U–U potential in a site–site intermolecular potential for UF_6 leads to unreasonably high values of the second virial coefficient, and to correspondingly high binding energies of the UF_6 dimer. Under the given circumstances we have resorted to fitting all the coefficients A_{ij}, B_{ij}, and C_{ij} for uranium with respect to the temperature dependence of the second virial coefficient of UF_6. Since the extensive report of Aziz and Taylor,[13] containing a well-documented comparison between the available isotropic intermolecular potentials for hexafluoride gases, provides an elaborate isotropic UF_6–UF_6 potential correlating second virial coefficient and viscosity data, we have chosen as reference for the temperature dependence of the second virial coefficient of UF_6 the recommended data of this report. We have also enlarged the data set to be reproduced by our site–site potential by including the equilibrium dimer separation (actually the U–U distance), as prescribed by the minimum position of the potential of Aziz and Taylor, which amounts to 5.381 Å.

Concerning the polarizabilities α_i appearing in the induction term U^{ind} given by Eq. (11), we use for fluorine the same values as in the case of SF_6.[7] As for uranium, we have considered a polarizability of 7.9338 Å^3, such as to reproduce the total UF_6 polarizability recommended by the Gmelin Handbook.[24]

All relevant data for the description of our potential models are summarized in Table III.

A few words are due to the evaluation of the second virial coefficient. The pair potential for two molecules is in general a function of 12 coordinates, three position coordinates and three Euler angles for each molecule. In a coordinate frame in which one of the molecules is placed unrotated at the origin, the second virial coefficient may be expressed as a sixfold integral over the relative position $\mathbf{r}\equiv(r,\theta,\varphi)$ and rotation $\mathbf{\Omega}\equiv(\Phi,\Theta,\Psi)$ of the second molecule:[25]

$$B(T)=-\frac{N_a}{16\pi^2}\int_0^\infty r^2dr\int_0^\pi\sin\theta d\theta\int_0^{2\pi}d\varphi\times\int_0^{2\pi}d\Phi\int_0^\pi\sin\Theta d\Theta\int_0^{2\pi}d\Psi\times\{\exp[-U(\mathbf{r},\mathbf{\Omega})/k_BT]-1\}.$$

For evaluation of the second virial coefficient of UF_6, we have employed the method of Stroud.[26] Taking advantage of the O_h symmetry of the UF_6 monomer, by halving each angular integration interval one can reduce the relevant space of relative orientations for two molecules, implying the positional (θ,φ)—and the Euler (Φ,Θ,Ψ) angles, by a factor of 32. To obtain our final results for the second virial coefficient, we have used an uniform spatial mesh, with the radial coordinate restricted to the interval [2,34] (Å), outside of which the integrand has been negligible for the considered potential models. The radial spacing has been taken equal to 2 Å, and the angular spacings equal to $\pi/8$, resulting in 13 107 200 integration points, which have been proved to ensure the convergence of the virial coefficient values with five exact digits for all temperatures.

In Fig. 1, the temperature dependence of the second virial coefficient resulting from potential I (plotted with continuous line) can be seen to fairly pass through the recommended values of Aziz and Taylor.[13] The corresponding curve for potential II cannot be practically distinguished. The relative root mean square deviation of our results amounts to 3.9%, underestimating by up to 9% the recommended values of Aziz and Taylor in the lower temperature region.

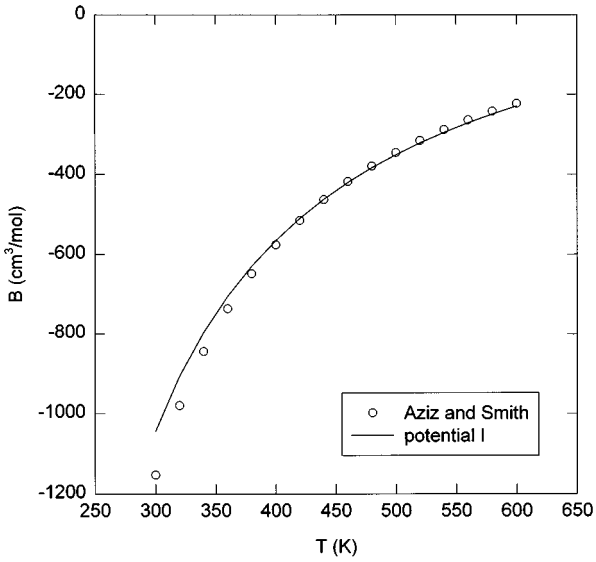

FIG. 1. Temperature dependence of the second virial coefficient of UF_6. With circles—the recommended values of Aziz and Taylor (Ref. 13); with continuous line—the dependence resulted using potential I.

C. Cluster structures

Taking into account the different nature of the interaction forces and the different orders of magnitude of the corresponding binding energies for the intra- and intermolecular degrees of freedom, in order to calculate the cluster structures we consider the molecules ''frozen'' in their equilibrium geometries and minimize the intermolecular potential with respect to their relative positions. Moreover, such a technique is consistent with the overall philosophy of our approach for frequency shifts. The positions and orientations of the molecules are specified by their center of mass Cartesian coordinates and Euler angles, which are optimized without constraints starting from randomly chosen initial configurations. Typically, several hundreds (for the dimer) up to 5–6 thousands (for the hexamer) of minimizations are required to yield the global minimum.

The results of our cluster structure calculations for potentials I and II are summarized in Table IV, where the binding energies and the mean U–U bond length of the clusters ranging from dimer to hexamer are listed. The mean U–U bond length is an indication of the ''compactness'' of the clusters. For all cluster sizes we have listed the data for the most stable (energetically lowest) isomer. Since, as will be later emphasized, the second and the third dimer configurations also show a remarkable symmetry, being energetically quite close to the most stable dimer, we have considered them too. The geometrical configurations of all the listed cluster structures are presented in Figs. 2–6. It should be noted that the cluster structures are alike for both discussed potential models.

TABLE IV. Calculated UF_6 cluster structures for the most stable isomers. E represents the total binding energy (in kJ/mol), and d_{UU} is the average U–U distance (in Å). The second and the third lowest dimer configurations ($2'$ and $2''$) are also included.

	Potential I		Potential II		
M	E	d_{UU}	E	d_{UU}	Symmetry
2	−8.66	5.381	−8.72	5.375	D_{2d}
$2'$	−7.84	5.469	−7.93	5.463	C_{2h}
$2''$	−7.69	5.312	−7.75	5.307	D_{3d}
3	−23.46	5.487	−23.74	5.477	D_3
4	−40.77	5.672	−41.20	5.666	C_3
5	−62.99	5.674	−63.41	5.669	C_{3h}
6	−86.17	5.741	−86.66	5.738	

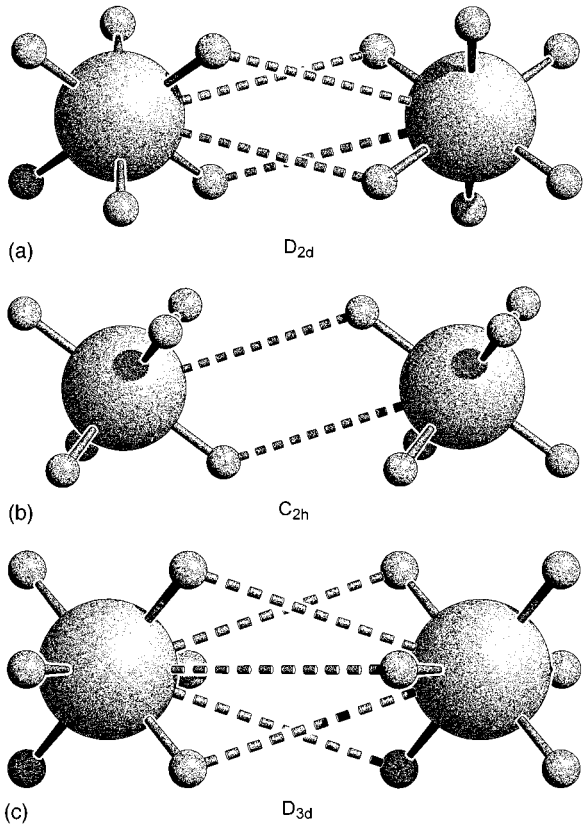

FIG. 2. Geometrical structures of the three dimer isomers found using potential I (D_{2d} is the lowest energy configuration). The shape of the corresponding isomers for potential II is identical.

We have depicted in Fig. 2 the three found dimers, the lowest having D_{2d} symmetry, the second (reduced) C_{2h} symmetry, and the third D_{3d} symmetry. Figure 3 shows the most stable trimer, exhibiting D_3 symmetry. Each monomer is connected to its neighbors by double U–F bonds, overlapping in the figure and providing a reminder of the double bond of the second lowest dimer.

The lowest tetramer, represented in Fig. 4, belongs to the C_3 point group, resembling the compact T_d symmetry arrangement of four rigid spheres. This resemblance is understandable having in view the huge size of the U atom, rendering the UF_6 molecule into an almost spherical structure. The most stable pentamer (Fig. 5) shows a well-defined (C_{3h}) symmetry, having a regular bi-pyramid shape, and this is again consistent with the fact that the uranium atom almost ''swallows'' the fluorine atoms.

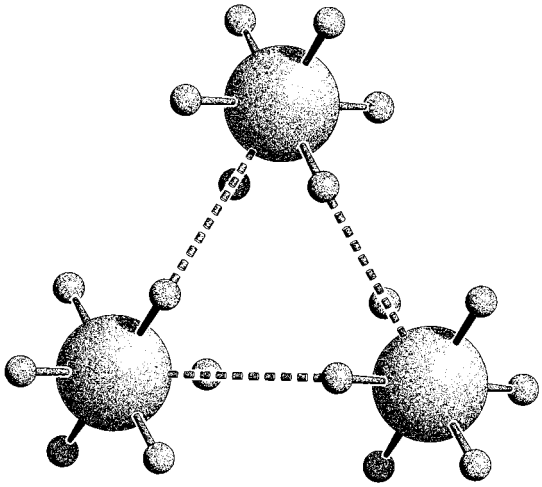

FIG. 3. Geometrical structure of the lowest trimer for potential I. Potential II yields an identically shaped trimer.

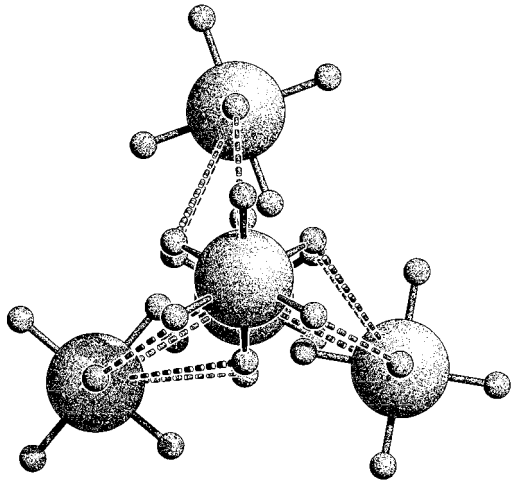

FIG. 5. Geometrical structure of the lowest pentamer for potential I. Potential II yields an identically shaped structure.

The most stable hexamer, depicted in Fig. 6, exhibits no particular symmetry. However, taking into account the quite close values of the in-plane distances between the U atoms contained in the ring and the out-of-plane U–U distances, it follows that the uranium atoms are organized according to a distorted O_h symmetry.

A general remark, which emerges from Table IV, is that for both potentials the binding energies never differ by more than 1%, with the corresponding average U–U distances differing even less (at most by 0.2%). This indicates that the induction contributions, which differentiate our two models, are not determining for the cluster structures. Thus, the geometrical size of the clusters shows little sensitivity to the electrostatic terms, evidencing the fact that UF_6 forms true van der Waals clusters, mainly bound by the dispersion attraction.

It is instructive to plot the incremental binding energy $E_M - E_{M-1}$ of the most stable isomers as a function of the cluster size M (Fig. 7). The hexamer does not conform to the general tendency of the curves, showing a reduced energy increment relative to the pentamer. This once more is a consequence of the reduced symmetry of the lowest hexamer.

D. Frequency shifts

In our band shift calculations for the UF_6 clusters, we have focused on the fundamental excitation of the ν_3 vibrational mode (at 627.724 cm^{-1}).

We have summarized in Table V the results of our frequency shift calculations for the most stable UF_6 dimer, both for potential I (including exchange, dispersion, and electrostatic terms) and potential II (additionally including induction contributions). As a result of the mutual interaction of the monomers within the dimer, the ν_3 vibrational mode is split up into a redshifted parallel band ($\parallel$) and a doubly degenerate blueshifted perpendicular band ($\perp$). The parallel

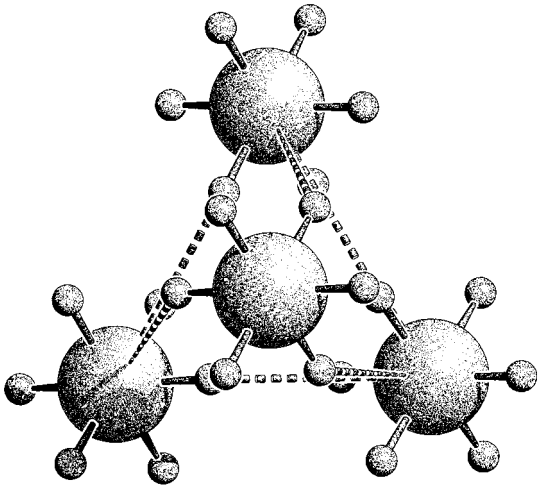

FIG. 4. Geometrical structure of the lowest tetramer for potential I. The shape resulted for potential II is identical.

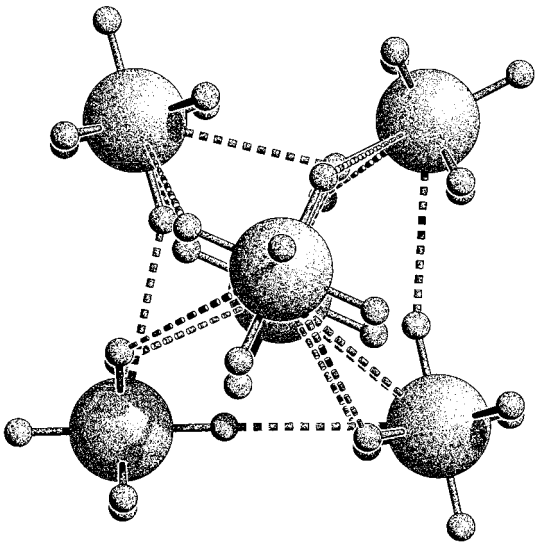

FIG. 6. Geometrical structure of the lowest hexamer for potential I. Potential II yields an identically shaped hexamer.

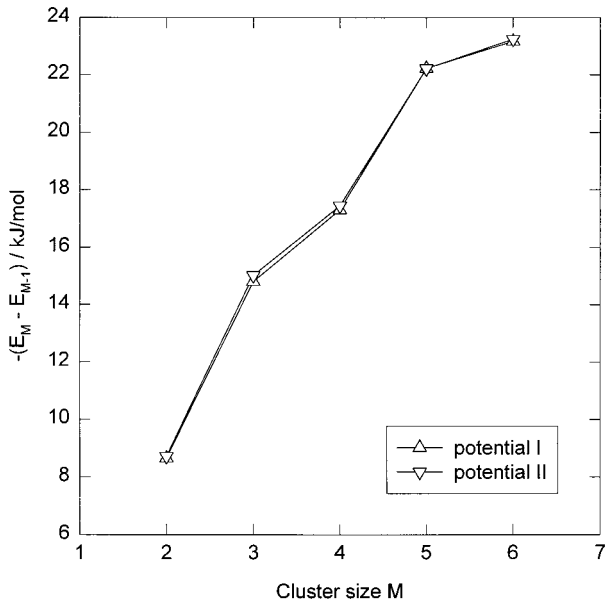

FIG. 7. Incremental binding energy of small UF_6 clusters.

band implies collective vibrations of the monomers along the longitudinal symmetry axis of the dimer, while for the perpendicular band, the resulting vibration takes place predominantly in a perpendicular plane. The differences between the line shifts corrected up to the second order and the first order results (added between parenthesis) represent the second order corrections, which typically amount to less than 0.5 cm^{-1}.

In order to identify the interaction mechanism which is mainly responsible for the frequency shifts, the individual contributions of the various potential terms to the line shifts have been evaluated by switching off the rest of the interactions, but considering the same dimer structure (obtained with the full potential model). It can be easily noticed that the electrostatic contributions are by far dominant, and by performing a molecular multipole analysis taking into account the O_h symmetry of the monomer, the vibrational dipole–dipole interaction turns out to be the leading mechanism. Furthermore, the effects of the exchange and dispersion couplings can be seen to be completely negligible. The induction, considered in potential II, contributes with up to 17% to the total frequency shifts, but as it will be further shown, its inclusion leads to a systematic redshift of the bands for all cluster sizes.

We have gathered in Table VI the calculated frequency shifts and line intensities for the UF_6 clusters up to the hexamer.

TABLE VI. Computed line shifts $\Delta\nu_3$ (in cm^{-1}), and total transition strengths $g|\mu_{01}|^2$ (in D^2) for UF_6 clusters up to the hexamer. g represents the degeneracy of the spectral line.

	Potential I		Potential II		
M	$\Delta\nu_3$	$g\|\mu_{01}\|^2$	$\Delta\nu_3$	$g\|\mu_{01}\|^2$	g
2	−7.14	0.28	−8.47	0.28	1
	4.69	0.56	4.14	0.56	2
3	−6.41	0.57	−7.61	0.57	2
	5.35	0.25	4.48	0.26	2
	10.68	0.42	8.62	0.42	1
4	−6.16	0.58	−7.41	0.56	2
	−5.66	0.31	−6.65	0.30	1
	9.30	0.53	7.23	0.55	2
	11.62	0.24	8.73	0.24	1
5	−6.08	0.21	−7.07	0.18	2
	−4.84	0.42	−5.73	0.43	2
	−4.62	0.59	−5.71	0.56	1
	7.70	0.11	5.65	0.14	1
	12.28	0.77	9.00	0.78	2
6	−4.54	0.30	−5.36	0.28	1
	−3.64	0.58	−4.68	0.54	1
	−3.42	0.58	−4.44	0.53	1
	8.30	0.46	6.28	0.45	1
	11.64	0.08	8.60	0.11	1
	13.24	0.25	9.14	0.28	1
	13.83	0.25	9.43	0.28	1

Figure 8 shows the stick spectra of the UF_6 clusters up to the hexamer, obtained by using potential I. The lines have been denoted according to the sign of the frequency shift: with $\parallel$ for redshifted lines and with $\perp$ for the blueshifted ones. While the ''parallel'' lines tend to preserve the red boundary of the spectra at about 623 cm^{-1} with increasing cluster size, the ''perpendicular'' lines gradually move toward higher frequencies, however with a saturation tendency, which brings about an almost non-varying total splitting when going from the tetramer to the pentamer. Apart from the supplementary splitting in the case of the tetramer, pentamer and hexamer, which is obviously due to the presence of monomers in non-equivalent positions, the parallel lines seem to be less sensitive to the ''compactness'' of the cluster (given by the average U–U distance) than the perpendicular lines.

TABLE V. Contributions of the various potential terms to the UF_6 dimer line shifts of the ν_3 mode (in cm^{-1}). Within parenthesis are given the first order results.

	Band	Exchange	Dispersion	Electrostatic	Induction	Total
Potential I	$\parallel$	0.12(0.12)	−0.06(−0.06)	−7.19(−7.57)		−7.14(−7.50)
	$\perp$	−0.01(0.00)	0.01(0.01)	4.68(4.53)		4.69(4.54)
Potential II	$\parallel$	0.12(0.12)	−0.06(−0.06)	−7.21(−7.59)	−1.46(−1.48)	−8.47(−9.00)
	$\perp$	−0.01(0.00)	0.01(0.01)	4.70(4.54)	−0.37(−0.37)	4.14(4.02)

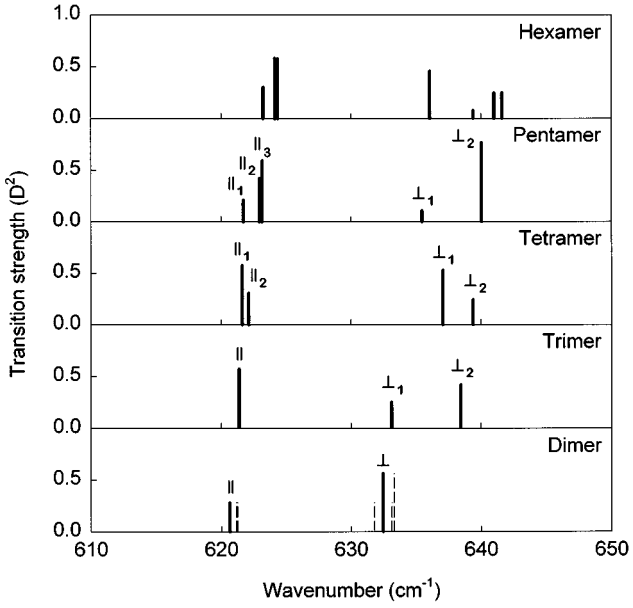

FIG. 8. Calculated stick spectra of UF_6 clusters from dimer to hexamer using potential I. The continuous lines correspond to the most stable isomers. The spectral lines for the second and third lowest dimer are plotted with dotted line.

As theoretical counterpart for our calculations, we have chosen the recent FTIR spectroscopy measurements of Tanimura *et al.*,[8] actually the only available experimental data about the UF_6 clusters. Figure 9 shows the FTIR spectra of the ν_3 band of UF_6 seeded in Ar at a mole fraction of 0.08 mol/mol and total pressures equal to 1.3, 3..0, and 5.0 Torr, along with the stick spectra for all cluster sizes up to the hexamer obtained with potential I. Figure 10 shows the same experimental spectra, along with the stick spectra obtained with potential II. As it can be seen from Fig. 9, the calculated stick spectrum for potential I reproduces the overall aspect of

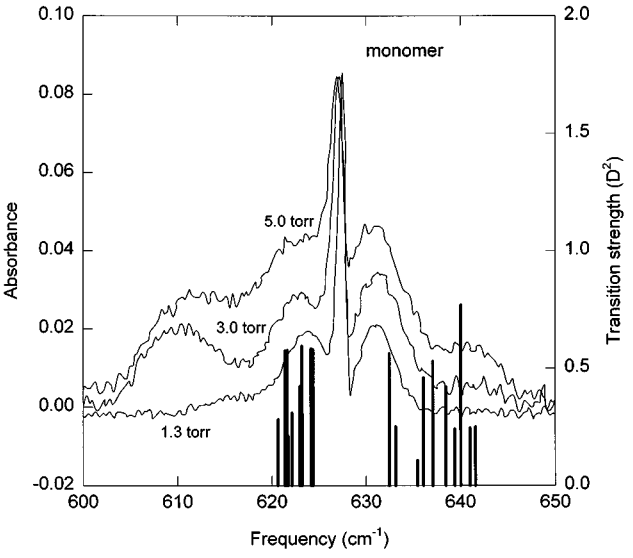

FIG. 9. FTIR spectra of UF_6 clusters (Ref. 8) and calculated stick spectra by using potential I.

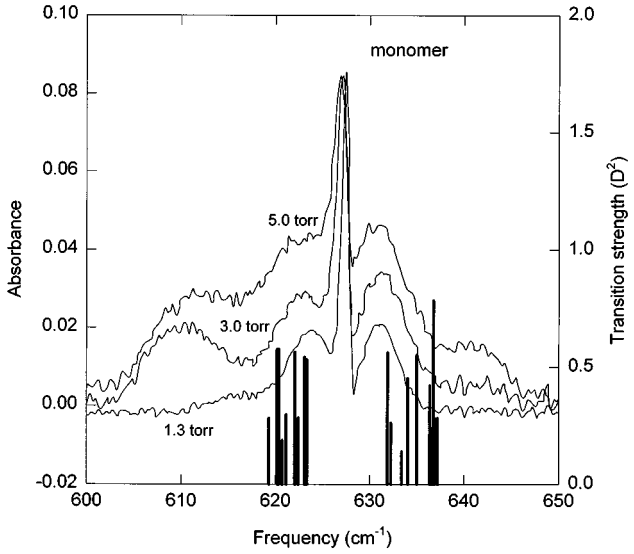

FIG. 10. FTIR spectra of UF_6 clusters (Ref. 8) and calculated stick spectra by using potential II.

the experimental bands situated around 623, 632 and 640 cm^{-1}. Whereas the peaks at 623 and 632 cm^{-1} also contain contributions from the P and R branches of the monomer spectrum, the peak at 640 cm^{-1} is clearly due to the presence of the UF_6 clusters solely, because it does not practically appear in the spectrum at 1.3 Torr. Since our calculations do not evidence dimer lines around 640 cm^{-1}, it follows that this peak should be attributed to the higher clusters (trimer, tetramer and so on), which are consequently formed only at total pressures above 3.0 Torr. It is also noteworthy that in the blueshifted band around 632 cm^{-1} there are only contributions from the dimer and the trimer, while in the redshifted band around 623 cm^{-1}, there are contributions from all cluster sizes. We did not find any theoretical line corresponding to the peak around 610 cm^{-1}, appearing in the FTIR spectrum at 3.0 Torr, but it is likely to be due to small UF_6–Ar clusters, even though the frequency of the ν_3 mode of UF_6 in Ar matrix has been reported to be 619.3 cm^{-1}.[27]

The theoretical stick spectrum obtained with potential II (Fig. 10), is more compact than the one for potential I and it is not organized into the three groups which have been attributed to the experimental bands situated around 623, 632 and 640 cm^{-1}. Hence, it seems that the inclusion of the induction interactions in our potential model worsens the agreement between the calculated spectrum and the experimental evidence. Consequently, it seems that the inclusion of the induction with the available polarizabilities is rather inappropriate.

IV. CONCLUSIONS

A new site–site intermolecular potential for UF_6, comprising exchange, dispersion, electrostatic, and induction contributions, is presented. The effective charges assigned to the U atom and the six additional ''electronic'' sites situated on the U–F bonds are chosen such as to account for the

observed vibrational transition dipole moment of the UF_6 monomer. The coefficients of the exp-6 part of the potential for uranium are determined by fitting the calculated temperature dependence of the second virial coefficient of UF_6 to the experimental evidence. Two variants of our potential model (one neglecting the induction interactions, and the other one including them) are applied to compute UF_6 cluster structures up to the hexamer. The average U–U distance and the incremental cluster binding energy are employed to correlate the ''compactness'' of the found cluster structures with their symmetry properties. It is shown that UF_6 forms true van der Waals clusters, mainly bound by the dispersion attraction, the effect of the induction interactions being negligible.

A second order line shift formalism is used to calculate the IR-spectra of the found UF_6 clusters in the region of the ν_3 vibrational mode. The contributions to the line shifts from the various interaction terms are analyzed and it is found that the electrostatic coupling is dominant. By a molecular multipole analysis, this large contribution can be attributed to the vibrational dipole–dipole interaction. The calculated spectra compare favorably with the available experimental FTIR spectra from the literature. The inclusion of the induction interaction produces a systematic redshift of the spectra for all cluster sizes and renders the inclusion of the induction interaction with the available atomic polarizabilities rather inappropriate.

ACKNOWLEDGMENTS

One of the authors (T.A.B) would like to express his thanks to Dr. S. Tanimura (RIKEN) for providing him with the experimental FTIR spectra prior to publication, and for explanations on the experimental techniques.

[1] J. Geraedts, S. Stolte, and J. Reuss, Z. Phys. A **304**, 167 (1982); J. Geraedts, M. Waayer, S. Stolte, and J. Reuss, Faraday Discuss. Chem. Soc. **73**, 375 (1982).
[2] M. Snels and R. Fantoni, Chem. Phys. **109**, 67 (1986); M. Snels and J. Reuss, Chem. Phys. Lett. **140**, 543 (1987).
[3] F. Huisken and M. Stemmler, Chem. Phys. **132**, 351 (1989).
[4] B. Heijmen, A. Bizzarri, S. Stolte, and J. Reuss, Chem. Phys. **132**, 331 (1989).
[5] J. W. I. van Bladel and A. van der Avoird, J. Chem. Phys. **92**, 2837 (1989).
[6] A. Boutin, J.-B. Maillet, and A. H. Fuchs, J. Chem. Phys. **99**, 9944 (1993); A. Boutin, B. Rousseau, and A. H. Fuchs, Chem. Phys. Lett. **218**, 122 (1994).
[7] T. A. Beu and K. Takeuchi, J. Chem. Phys. **103**, 6394 (1995).
[8] S. Tanimura, Y. Okada, and K. Takeuchi, J. Phys. Chem. **100**, 2842 (1996).
[9] J. A. Barnes and T. E. Gough, Chem. Phys. Lett. **130**, 297 (1986); J. Chem. Phys. **86**, 6012 (1987).
[10] A. D. Buckingham, Proc. R. Soc. London, Ser. A **248**, 169 (1958); *ibid.*, **255**, 32 (1960); Trans. Faraday Soc. **56**, 753 (1960).
[11] K. C. Kim and W. B. Person, J. Chem. Phys. **74**, 171 (1981).
[12] M. Pepper and B. E. Bursten, J. Am. Chem. Soc. **112**, 7803 (1990).
[13] R. A. Aziz and W. L. Taylor, *Final Report: Intermolecular Potentials for Hexafluoride Gases*, MLM-3611, Oct. 31, 1989, for the U.S. Department of Energy, Contract No. DE-AC04-88DP43495.
[14] A. Dalgarno, in *Quantum Theory*, edited by D. R. Bates (Academic, New York, 1961).
[15] E. B. Wilson, J. C. Decius, and P. C. Cross, *Molecular Vibrations* (McGraw-Hill, New York, 1955).
[16] G. Herzberg, *Molecular Spectra and Molecular Structure. II. Infrared and Raman Spectra of Polyatomic Molecules* (Van Nostrand, Toronto, 1945) p. 123.
[17] C. W. F. T. Pistorius, J. Chem. Phys. **29**, 1328 (1958).
[18] J. P. Aldridge *et al.*, J. Chem. Phys. **83**, 34 (1985).
[19] L. Hedberg and I. M. Mills, J. Mol. Spectrosc. **160**, 117 (1993).
[20] A. R. Hoy, I. M. Mills, and G. Strey, Mol. Phys. **24**, 1265 (1972).
[21] J. Onoe *et al.*, J. Chem. Phys. **99**, 6810 (1993).
[22] M. A. Spackman, J. Chem. Phys. **85**, 6579 (1986).
[23] R. G. Gordon and Y. S. Kim, J. Chem. Phys. **56**, 3122 (1972).
[24] Gmelin Handbuch der Anorganischen Chemie, 8th ed., Uranium Suppl. Vol. C8, 1980.
[25] J. O. Hirschfelder, C. F. Curtiss, and R. B. Bird, *Molecular Theory of Gases and Liquids* (Wiley, New York, 1954).
[26] A. H. Stroud, *Approximate Calculation of Multiple Integrals* (Prentice-Hall, Englewood Cliffs, 1971).
[27] R. T. Paine *et al.*, J. Chem. Phys. **64**, 3081 (1976).